AIAA JOURNAL
Vol. 34, No. 1, January 1996

Analysis of Piezoelastic Structures with Laminated Piezoelectric Triangle Shell Elements

H. S. Tzou* and R. Ye†
University of Kentucky, Lexington, Kentucky 40506-0108

In the recent development of active structural systems and microelectromechanical systems, piezoelectrics are widely used as sensors and actuators. Because of the limitations of theoretical and experimental models in design applications, finite element development and analysis are proposed and presented in this paper. A new laminated quadratic C^0 piezoelastic triangular shell finite element is developed using the layerwise constant shear angle theory. Element and system equations are also derived. The developed piezoelastic triangular shell element is used to model 1) a piezoelectric bimorph pointer and 2) a semicircular ring shell. Finite element (triangular shell finite element) solutions are compared closely with the theoretical, experimental, and finite element (thin solid finite element) results in the bimorph pointer case. Natural frequencies and distributed control effects of the ring shell with piezoelectric actuators of various length are also studied. Finite element analyses suggested that the inherent piezoelectric effect has little effect on natural frequencies of the ring shell. Vibration control effect increases as the actuator length increases, and it starts leveling off at the seven-patch (70%) actuator. Coupling and control spillover of lower natural modes are also observed.

Introduction

IN the recent development of active intelligent structural systems and microelectromechanical systems, piezoelectrics are very popular in both sensor and actuator applications because of their inherent electromechanical characteristics: the direct and converse piezoelectric effects. Studies of piezoelectricity were pioneered by the Curie brothers in 1880 and have been continuously advanced over the years.[1] Applications of piezoelectric materials as distributed sensors and actuators in active structural systems were proposed and intensively investigated in recent years. It is generally recognized that theoretical models are effective only to very limited well-defined geometries and boundary conditions. On the other hand, experimental models and prototypes are limited to relatively simple structures, such as beams (mostly) and plates (some). In practical applications, finite element (FE) techniques provide the versatilities in modeling, simulation, and analysis of engineering designs in modern industries.

Isoparametric piezoelectric hexahedron and tetrahedron FEs were developed and used in piezoceramic transducer designs.[2,3] A piezoelectric beam FE was used in distributed vibration control of a lead zirconate titanate (PZT)–steel laminated beam.[4] Tzou and Tseng[5] proposed a nonconforming thin piezoelectric hexahedron FE with three internal degrees of freedom and studied distributed sensing and vibration control of layered plates. Ha et al.[6] derived an eight-node composite brick element. Hwang and Park[7] developed a piezoelectric plate element and compared their results with published data. Rao and Sunar[8] proposed a thermopiezoelectric element. Layerwise piezoelectric theories and structures were recently studied.[9,10] Tzou and Ye[11] also derived a three-dimensional thin piezothermoelastic element and examined the piezothermoelasticity and control effects of piezoelectric systems. This paper is concerned with a new development of a laminated quadratic C^0 piezoelastic triangular shell FE and its applications to precision manipulation and vibration control.

Classical plate or shell theory is based on either a classical lamination theory (Love–Kirchhoff hypothesis) or a constant shear-angle theory (Reissner–Mindlin hypothesis). In recent years, intensive studies of static and dynamic analyses of thin or thick shell structures indicate that the classical plate or shell theory overpredicts the natural frequency and underpredicts the deflection and specific damping capacity.[12] This is due to neglecting the effects of transverse shear, thickness lamination, and a high degree of anisotropy of the laminated anisotropic plates and shells. Accordingly, many improved theories including these effects have been proposed.[12–14] One of them, called the layerwise constant shear angle theory,[15] is used in this research, which accounts for a layerwise constant approximation of the nonlinear cross-sectional warping. Detailed FE formulation of a laminated piezoelastic shell FE, based on the layerwise constant shear angle theory, is presented, and applications to distributed sensing and control of piezoelectric laminated structures are demonstrated.

Received Sept. 6, 1994; revision received Feb. 24, 1995; accepted for publication Feb. 25, 1995.

*Associate Professor, Department of Mechanical Engineering.
†Research Assistant, Department of Mechanical Engineering and Center for Computational Sciences.

Piezoelastic Laminated Shells

A laminated piezoelastic shell continuum is composed of N laminae which could be either elastic materials or piezoelastic materials, Fig. 1. It is assumed that the piezoelectric laminate is exposed to a displacement field and an electric field. For a conservative field, e.g., the displacement or electric field, a minimum potential energy functional can be directly established from the virtual work principal. Thus, energy functionals denoted by $\mathcal{F}_u$ and $\mathcal{F}_\phi$ for the displacement and electric fields can be expressed as

$$\mathcal{F}_u(u) = \int_V \left(\frac{1}{2} c_{ijkl} S_{ij} S_{kl} - e_{mij} E_m S_{ij}\right) \mathrm{d}V - \int_{S_T} f_i u_i \, \mathrm{d}S - \int_V (f_{bi} - \rho \ddot{u}_i) u_i \, \mathrm{d}V \tag{1}$$

$$\mathcal{F}_\phi(\phi) = \int_V \left[\frac{1}{2} \epsilon_{ij} E_i E_j + e_{ijk} E_i S_{jk}\right] \mathrm{d}V - \int_{S_D} \phi Q \, \mathrm{d}S \tag{2}$$

where c_{ijkl} are the elastic moduli, S_{ij} the displacement components, e_{mij} the piezoelectric coefficients, E_m the electric fields, f_i

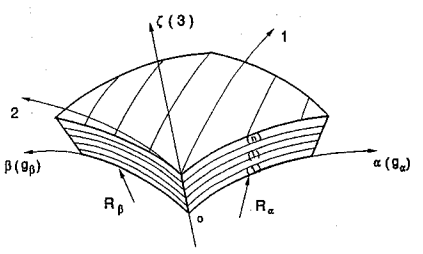

Fig. 1 Laminated shell and its coordinate system.

the excitation forces, u_i the displacement components, f_{bi} the body forces. Also, ρ is the mass density, $\ddot{u}_i$ denote the acceleration components, ϵ_{ij} are the dielectric constants or permittivities, ϕ is the electric potential, and Q is the surface charge. V is the volume of the piezoelastic continuum, and S_T and S_D are the boundary surface specified by the surface force vector f_i and charge Q. Taking variations with respect to the independent variables u_i and ϕ in the functionals $\mathcal{F}_u(u)$ and $\mathcal{F}_\phi(\phi)$, one can derive the stationary conditions for the piezoelastic continuum, i.e., the equilibrium equations, electrostatic equation, and boundary conditions.[11]

All relations of displacement, strain, stress, electric field, and electric potential are established in an orthogonal curvilinear coordinate system (α, β, ζ). Note that the curvilinear coordinates α and β usually correspond to the lines of principal curvature on the surface parallel the neutral surface of the shell, and ζ is measured along the normal to the α–β surface. Here, for convenience, the α and β coordinates are placed on the bottom surface of the shell.

Considering small deformations of the laminated piezoelastic shell, one can derive the strain-displacement and electric field–electric potential equations[1]:

$$S_\alpha(\zeta) = \frac{1}{[1+(\zeta/R_\alpha)]g_\alpha}\left[\frac{\partial u_\alpha(\zeta)}{\partial\alpha} + \frac{1}{g_\beta}\frac{\partial g_\alpha}{\partial\beta}u_\beta(\zeta) + \frac{g_\alpha}{R_\alpha}w(\zeta)\right] \tag{3}$$

$$S_\beta(\zeta) = \frac{1}{[1+(\zeta/R_\beta)]g_\beta}\left[\frac{\partial u_\beta(\zeta)}{\partial\beta} + \frac{1}{g_\alpha}\frac{\partial g_\beta}{\partial\beta}u_\alpha(\zeta) + \frac{g_\beta}{R_\beta}w(\zeta)\right] \tag{4}$$

$$S_\zeta(\zeta) = \frac{\partial w(\zeta)}{\partial\zeta} \tag{5}$$

$$S_{\alpha\beta}(\zeta) = \frac{1}{[1+(\zeta/R_\alpha)]g_\alpha}\left[\frac{\partial u_\beta(\zeta)}{\partial\alpha} - \frac{1}{g_\beta}\frac{\partial g_\alpha}{\partial\beta}u_\alpha(\zeta)\right] + \frac{1}{[1+(\zeta/R_\beta)]g_\beta}\left[\frac{\partial u_\alpha(\zeta)}{\partial\beta} - \frac{1}{g_\alpha}\frac{\partial g_\beta}{\partial\alpha}u_\beta(\zeta)\right] \tag{6}$$

$$S_{\alpha\zeta}(\zeta) = \frac{1}{[1+(\zeta/R_\alpha)]g_\alpha}\left[\frac{\partial w(\zeta)}{\partial\alpha} - \frac{g_\alpha}{R_\alpha}u_\alpha(\zeta)\right] + \frac{\partial u_\alpha(\zeta)}{\partial\zeta} \tag{7}$$

$$S_{\beta\zeta}(\zeta) = \frac{1}{[1+(\zeta/R_\beta)]g_\beta}\left[\frac{\partial w(\zeta)}{\partial\beta} - \frac{g_\beta}{R_\beta}u_\beta(\zeta)\right] + \frac{\partial u_\beta(\zeta)}{\partial\zeta} \tag{8}$$

$$E_\alpha(\zeta) = -\frac{1}{[1+(\zeta/R_\alpha)]g_\alpha}\frac{\partial\phi(\zeta)}{\partial\alpha} \tag{9}$$

$$E_\beta(\zeta) = -\frac{1}{[1+(\zeta/R_\beta)]g_\beta}\frac{\partial\phi(\zeta)}{\partial\beta} \tag{10}$$

$$E_\zeta(\zeta) = -\frac{\partial\phi(\zeta)}{\partial\zeta} \tag{11}$$

where R_α and R_β are the radii of principal curvature; g_α and g_β are the Lamé parameters; $u_\alpha(\zeta)$, $u_\beta(\zeta)$, and $w(\zeta)$ are the displacements in the α, β, and ζ directions; $S_x(\zeta)$ and $S_{xy}(\zeta)$, $(x, y = \alpha, \beta, \zeta)$ are the normal and shear strain components, respectively; $\phi(\zeta)$ is the electric potential; and $E_\alpha(\zeta)$, $E_\beta(\zeta)$, and $E_\zeta(\zeta)$ are the electric fields in the α, β, and ζ directions, respectively. It is assumed that the piezoelastic material is made of class-mm2 piezoelectrics,[16] where the first m implies that the material possesses a plane of symmetry perpendicular to the α axis, the second m denotes a plane of symmetry perpendicular to the β axis, and the final 2 means that the ζ axis is a two-fold rotation axis. Thus, the constitutive relations of a piezoelectric layer, referring to an arbitrary orthogonal curvilinear coordinate (α, β, ζ), are

$$\begin{Bmatrix} T_\alpha(\zeta) \\ T_\beta(\zeta) \\ T_\zeta(\zeta) \\ T_{\alpha\beta}(\zeta) \\ T_{\alpha\zeta}(\zeta) \\ T_{\beta\zeta}(\zeta) \end{Bmatrix} = \begin{bmatrix} \bar{c}_{11} & \bar{c}_{12} & \bar{c}_{13} & \bar{c}_{14} & 0 & 0 \\ & \bar{c}_{22} & \bar{c}_{23} & \bar{c}_{24} & 0 & 0 \\ & & \bar{c}_{33} & \bar{c}_{34} & 0 & 0 \\ & & & \bar{c}_{44} & 0 & 0 \\ & \text{(sym.)} & & & \bar{c}_{55} & \bar{c}_{56} \\ & & & & & \bar{c}_{66} \end{bmatrix} \begin{Bmatrix} S_\alpha(\zeta) \\ S_\beta(\zeta) \\ S_\zeta(\zeta) \\ S_{\alpha\beta}(\zeta) \\ S_{\alpha\zeta}(\zeta) \\ S_{\beta\zeta}(\zeta) \end{Bmatrix} - \begin{bmatrix} 0 & 0 & \bar{e}_{31} \\ 0 & 0 & \bar{e}_{32} \\ 0 & 0 & \bar{e}_{33} \\ 0 & 0 & \bar{e}_{34} \\ \bar{e}_{15} & \bar{e}_{25} & 0 \\ \bar{e}_{16} & \bar{e}_{26} & 0 \end{bmatrix} \begin{Bmatrix} E_\alpha(\zeta) \\ E_\beta(\zeta) \\ E_\zeta(\zeta) \end{Bmatrix} \tag{12}$$

$$\begin{Bmatrix} D_\alpha(\zeta) \\ D_\beta(\zeta) \\ D_\zeta(\zeta) \end{Bmatrix} = \begin{bmatrix} 0 & 0 & 0 & 0 & \bar{e}_{15} & \bar{e}_{16} \\ 0 & 0 & 0 & 0 & \bar{e}_{25} & \bar{e}_{26} \\ \bar{e}_{31} & \bar{e}_{32} & \bar{e}_{33} & \bar{e}_{34} & 0 & 0 \end{bmatrix} \begin{Bmatrix} S_\alpha(\zeta) \\ S_\beta(\zeta) \\ S_\zeta(\zeta) \\ S_{\alpha\beta}(\zeta) \\ S_{\alpha\zeta}(\zeta) \\ S_{\beta\zeta}(\zeta) \end{Bmatrix} + \begin{bmatrix} \bar{\epsilon}_{11} & \bar{\epsilon}_{12} & 0 \\ \bar{\epsilon}_{12} & \bar{\epsilon}_{22} & 0 \\ 0 & 0 & \bar{\epsilon}_{33} \end{bmatrix} \begin{Bmatrix} E_\alpha(\zeta) \\ E_\beta(\zeta) \\ E_\zeta(\zeta) \end{Bmatrix} \tag{13}$$

where $T_x(\zeta)$ and $T_{xy}(\zeta)$ $(x, y = \alpha, \beta, \zeta)$ denote the stress components; $D_\alpha(\zeta)$, $D_\beta(\zeta)$, and $D_\zeta(\zeta)$ are the electric displacements. For an arbitrary layer i $(i = 1, 2, \ldots, N)$, strain, electric-field, stress, and electric-displacement equations can be simply written as

$$\{S^{(i)}(\zeta)\} = [L_u^{(i)}]\{u^{(i)}(\zeta)\} \tag{14}$$

$$\{E^{(i)}(\zeta)\} = -[L_\phi^{(i)}]\phi^{(i)}(\zeta) \tag{15}$$

$$\{T^{(i)}(\zeta)\} = [\bar{c}^{(i)}]\{S^{(i)}(\zeta)\} - [\bar{e}^{(i)}]\{E^{(i)}(\zeta)\} \tag{16}$$

$$\{D^{(i)}(\zeta)\} = [\bar{e}^{(i)}]^t\{S^{(i)}(\zeta)\} + [\bar{\epsilon}^{(i)}]\{E^{(i)}(\zeta)\} \tag{17}$$

where strain $\{S^{(i)}(\zeta)\} = \{S_\alpha^{(i)}(\zeta), S_\beta^{(i)}(\zeta), S_\zeta^{(i)}(\zeta), S_{\alpha\beta}^{(i)}(\zeta), S_{\alpha\zeta}^{(i)}(\zeta), S_{\beta\zeta}^{(i)}(\zeta)\}^t$; displacement $\{u^{(i)}(\zeta)\} = \{u_\alpha^{(i)}(\zeta), u_\beta^{(i)}(\zeta), w^{(i)}(\zeta)\}^t$; electric field $\{E^{(i)}(\zeta)\} = \{E_\alpha^{(i)}(\zeta), E_\beta^{(i)}(\zeta), E_\zeta^{(i)}(\zeta)\}^t$; stress $\{T^{(i)}(\zeta)\} = \{T_\alpha^{(i)}(\zeta), T_\beta^{(i)}(\zeta), T_\zeta^{(i)}(\zeta), T_{\alpha\beta}^{(i)}(\zeta), T_{\alpha\zeta}^{(i)}(\zeta), T_{\beta\zeta}^{(i)}(\zeta)\}^t$; electric displacement $\{D^{(i)}(\zeta)\} = \{D_\alpha^{(i)}(\zeta), D_\beta^{(i)}(\zeta), D_\zeta^{(i)}(\zeta)\}^t$; the superscript t denotes the matrix/vector transpose; and $[L_u^{(i)}]$ and $[L_\phi^{(i)}]$ are the differential operator matrices defined by

$$[L_u^{(i)}] = \left[\begin{array}{ccc|c|c|c} \mathcal{B}_\alpha\frac{\partial}{\partial\alpha} & \frac{\mathcal{B}_\beta}{g_\alpha}\frac{\partial g_\beta}{\partial\beta} & 0 & \mathcal{B}_\beta\frac{\partial}{\partial\beta} - \frac{\mathcal{B}_\alpha}{g_\beta}\frac{\partial g_\alpha}{\partial\beta} & \frac{\partial}{\partial\zeta} - \frac{1}{B_\alpha R_\alpha} & 0 \\ \frac{\mathcal{B}_\alpha}{g_\beta}\frac{\partial g_\alpha}{\partial\alpha} & \mathcal{B}_\beta\frac{\partial}{\partial\beta} & 0 & \mathcal{B}_\alpha\frac{\partial}{\partial\alpha} - \frac{\mathcal{B}_\beta}{g_\alpha}\frac{\partial g_\beta}{\partial\alpha} & 0 & \frac{\partial}{\partial\zeta} - \frac{1}{B_\beta R_\beta} \\ \frac{1}{B_\alpha R_\alpha} & \frac{1}{B_\beta R_\beta} & \frac{\partial}{\partial\zeta} & 0 & \mathcal{B}_\alpha\frac{\partial}{\partial\alpha} & \mathcal{B}_\beta\frac{\partial}{\partial\beta} \end{array}\right]^t \tag{18}$$

$$\left[L_\phi^{(i)}\right] = \left[\mathcal{B}_\alpha \frac{\partial}{\partial \alpha} \,\middle|\, \mathcal{B}_\beta \frac{\partial}{\partial \beta} \,\middle|\, \frac{\partial}{\partial \zeta}\right]^t \tag{19}$$

where

$$B_\alpha = 1 + \frac{\zeta}{R_\alpha}, \qquad B_\beta = 1 + \frac{\zeta}{R_\beta}$$

$$\mathcal{B}_\alpha = \frac{1}{B_\alpha g_\alpha}, \qquad \mathcal{B}_\beta = \frac{1}{B_\beta g_\beta}$$

Finite Element Formulation

The assumption of layerwise constant shear angle is used in the FE derivation. That is, the straight lines in each layer normal to the undeformed shell remain straight, but they rotate with respect to the normal to the deformed shell by an amount that varies from layer to layer. A quadratic C° piezoelastic triangular shell FE with 12 nodes, four degrees of freedom $(u_\alpha, u_\beta, w, \phi)$ per node, is derived. The element is quadratic in two in-plane axes and linear in the transverse direction. The ith layer triangular shell element is bounded by the ith and $(i+1)$th interfaces; the interface triangle is characterized by six nodes, one at each triangular corner, and one at the center of each side on the interface plane parallel to the $\alpha\beta$ plane. Figure 2 illustrates the triangular shell element.

Thus, the displacement and electric fields $u_\alpha^{(i)}(\zeta)$, $u_\beta^{(i)}(\zeta)$, $w^{(i)}(\zeta)$, and $\phi^{(i)}(\zeta)$ for the arbitrary ith layer can be expressed as

$$u_\alpha^{(i)}(\zeta) = \bar{u}_\alpha^{(i)}(1 - \zeta/h_i) + \bar{u}_\alpha^{(i+1)}\zeta/h_i \tag{20}$$

$$u_\beta^{(i)}(\zeta) = \bar{u}_\beta^{(i)}(1 - \zeta/h_i) + \bar{u}_\beta^{(i+1)}\zeta/h_i \tag{21}$$

$$w^{(i)}(\zeta) = \bar{w}^{(i)}(1 - \zeta/h_i) + \bar{w}^{(i+1)}\zeta/h_i \tag{22}$$

$$\phi^{(i)}(\zeta) = \bar{\phi}^{(i)}(1 - \zeta/h_i) + \bar{\phi}^{(i+1)}\zeta/h_i \quad i = 1, 2, \ldots, N \tag{23}$$

or simply written as

$$\left\{u^{(i)}(\zeta)\right\} = \left[N_u^{(i)}(\zeta)\right]\left\{\bar{u}^{(i)}\right\} \tag{24}$$

$$\phi^{(i)}(\zeta) = \left[N_\phi^{(i)}(\zeta)\right]\left\{\bar{\phi}^{(i)}\right\} \tag{25}$$

where $\{\bar{u}^{(i)}\} = \{\bar{u}_\alpha^{(i)}, \bar{u}_\beta^{(i)}, \bar{w}^{(i)}, \bar{u}_\alpha^{(i+1)}, \bar{u}_\beta^{(i+1)}, \bar{w}^{(i+1)}\}$, and $\{\bar{\phi}^{(i)}\} = \{\bar{\phi}^{(i)}, \bar{\phi}^{(i+1)}\}$ are the displacement and electric potential vectors of the ith and $(i+1)$th interfaces along the curvilinear coordinate axes; $[N_u^{(i)}(\zeta)]$ and $[N_\phi^{(i)}(\zeta)]$ are the shape functions in terms of the coordinate ζ; and h_i is the thickness of the ith layer. Note that the coordinate ζ now is local to each layer. Furthermore, the surface parallel displacements and electric potential in each triangular region at the ith interface can be interpolated by the nodal degree of freedom, that is,

$$\bar{u}_\alpha^{(i)} = \{N\}^t\left\{u_\alpha^{(i)}\right\} \tag{26}$$

$$\bar{u}_\beta^{(i)} = \{N\}^t\left\{u_\beta^{(i)}\right\} \tag{27}$$

$$\bar{w}^{(i)} = \{N\}^t\left\{w^{(i)}\right\} \tag{28}$$

$$\bar{\phi}^{(i)} = \{N\}^t\left\{\phi^{(i)}\right\} \tag{29}$$

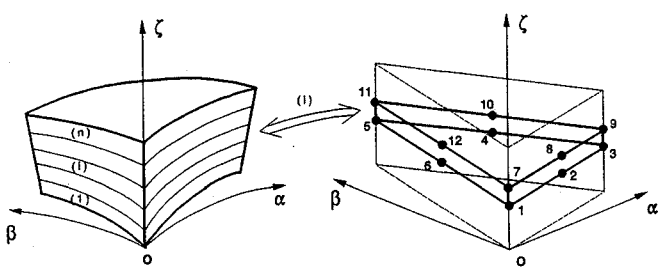

Fig. 2 Laminated triangular shell element.

where $\{u_\alpha^{(i)}\} = \{u_{\alpha 1}^i, \ldots, u_{\alpha 6}^i\}^t$, $\{u_\beta^{(i)}\} = \{u_{\beta 1}^i, \ldots, u_{\beta 6}^i\}^t$, $\{w^{(i)}\} = \{w_1^i, \ldots, w_6^i\}^t$, and $\{\phi^{(i)}\} = \{\phi_1^i, \ldots, \phi_6^i\}^t$ are the nodal displacements and nodal electric potential of the element at the ith interface, respectively; and $\{N\}^t = \{\xi_1(2\xi_1 - 1), 4\xi_1\xi_2, \xi_2(2\xi_2 - 1), 4\xi_2\xi_3, \xi_3(2\xi_3 - 1), 4\xi_3\xi_1\}$ are the shape function expressed by area coordinates.[17] Substituting Eqs. (26–29) into Eqs. (24) and (25) leads to the following expressions of displacement $\{\bar{u}^{(i)}\}$ and potential $\{\bar{\phi}^{(i)}\}$:

$$\left\{\bar{u}^{(i)}\right\} = \left[N_{u_j}(\alpha, \beta)\right]\left\{u_j^{(i)}\right\} \tag{30}$$

$$\left\{\bar{\phi}^{(i)}\right\} = \left[N_{\phi_j}(\alpha, \beta)\right]\left\{\phi_j^{(i)}\right\} \tag{31}$$

where $\{u_j^{(i)}\} = \{u_{\alpha 1}^i, u_{\beta 1}^i, w_1^i, \ldots, u_{\alpha 6}^i, u_{\beta 6}^i, w_6^i, u_{\alpha 1}^{i+1}, u_{\beta 1}^{i+1}, w_1^{i+1}, \ldots, u_{\alpha 6}^{i+1}, u_{\beta 6}^{i+1}, w_6^{i+1}\}^t$ and $\{\phi_j^{(i)}\} = \{\phi_1^i, \ldots, \phi_6^i, \phi_1^{i+1}, \ldots, \phi_6^{i+1}\}^t$ are the nodal displacements and nodal electric potential of the jth planar layer element located in the ith (thickness direction) layer, respectively; and $[N_{u_j}(\alpha, \beta)]$ and $[N_{\phi_j}(\alpha, \beta)]$ are the shape functions of coordinates α and β. Writing Eqs. (14) and (15) in terms of nodal variables of the element gives

$$\begin{aligned}\left\{S^{(i)}(\zeta)\right\} &= \left[L_u^{(i)}\right]\left[N_u^{(i)}(\zeta)\right]\left[N_{u_j}(\alpha, \beta)\right]\left\{u_j^{(i)}\right\} \\ &= \left[B_u^{(i)}(\zeta)\right]\left[B_{u_j}(\alpha, \beta)\right]\left\{u_j^{(i)}\right\}\end{aligned} \tag{32}$$

$$\begin{aligned}\left\{E^{(i)}(\zeta)\right\} &= -\left[L_\phi^{(i)}\right]\left[N_\phi^{(i)}(\zeta)\right]\left[N_{\phi_j}(\alpha, \beta)\right]\left\{\phi_j^{(i)}\right\} \\ &= -\left[B_\phi^{(i)}(\zeta)\right]\left[B_{\phi_j}(\alpha, \beta)\right]\left\{\phi_j^{(i)}\right\}\end{aligned} \tag{33}$$

Substituting Eqs. (16) and (17), (24) and (25), and (30–33) into Eqs. (1) and (2), and taking variations with respect to the nodal variables, one can derive the nodal governing equations of the jth (planar) layer element located in the ith (thickness) layer in a matrix representation,

$$\begin{bmatrix} \left[M_{uu_j}^{(i)}\right] & 0 \\ 0 & 0 \end{bmatrix} \begin{Bmatrix} \{\ddot{u}_j^{(i)}\} \\ \{\ddot{\phi}_j^{(i)}\} \end{Bmatrix} + \begin{bmatrix} \left[C_{uu_j}^{(i)}\right] & 0 \\ 0 & 0 \end{bmatrix} \begin{Bmatrix} \{\dot{u}_j^{(i)}\} \\ \{\dot{\phi}_j^{(i)}\} \end{Bmatrix}$$

$$+ \begin{bmatrix} \left[K_{uu_j}^{(i)}\right] & \left[K_{u\phi_j}^{(i)}\right] \\ \left[K_{\phi u_j}^{(i)}\right] & \left[K_{\phi\phi_j}^{(i)}\right] \end{bmatrix} \begin{Bmatrix} \{u_j^{(i)}\} \\ \{\phi_j^{(i)}\} \end{Bmatrix} = \begin{Bmatrix} \{F_{u_j}^{(i)}\} \\ \{F_{\phi_j}^{(i)}\} \end{Bmatrix} \tag{34}$$

where $[M_{uu_j}^{(i)}]$ is the mass matrix; $[C_{uu_j}^{(i)}]$ is the damping matrix; $[K_{uu_j}^{(i)}]$, $[K_{u\phi_j}^{(i)}]$, $[K_{\phi u_j}^{(i)}]$, and $[K_{\phi\phi_j}^{(i)}]$ are the stiffness matrices defined for the displacement and electric potential fields; and $\{F_{u_j}^{(i)}\}$ and $\{F_{\phi_j}^{(i)}\}$ are the mechanical and electric excitation. Detailed definitions of the element matrices are presented in the Appendix. Assembling the element matrices yields the system matrices and, accordingly, sensing and control of piezoelastic structures and systems can be proceeded.[1,5,11]

Numerical Examples

There are two cases presented in this section. The first is to validate the new piezoelastic triangular shell FE, and the second is to evaluate distributed control of a semicircular ring shell.

Case 1: Validation: Bimorph Pointer

A piezoelectric bimorph point is made of two piezoelectric layers laminated together with opposite polarity. This bimorph pointer can be used for microactuation, indication, and manipulation in high-precision operations.[18] Figure 3 illustrates the piezoelectric bimorph pointer and its triangular FE mesh distribution.

In this case, FE solutions of the piezoelectric bimorph pointer are compared with theoretical solutions[18] and laboratory experiments.[1] Static deflections induced by externally applied voltages are calculated using the newly developed FE program. Figure 4 shows the static beam deflection along the beam length indicated by node numbers; the fixed end has zero deflection and the free end has the maximal deflection. Note that the FE solutions are slightly lower

Table 1 Nodal displacements of the piezoelectric bimorph pointer, 10^{-7}m

Nodes	1	2	3	4	5
Theory	0.138	0.552	1.24	2.21	3.45
Solid FE	0.124	0.508	1.16	2.10	3.30
(Error %)	(10.1)	(8.0)	(6.5)	(5.0)	(4.3)
Shell FE	0.132	0.528	1.19	2.11	3.30
(Error %)	(4.3)	(4.3)	(4.0)	(4.5)	(4.3)

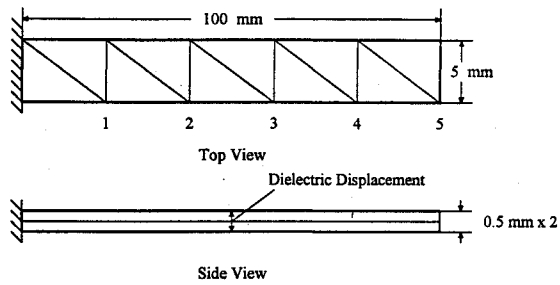

Fig. 3 Piezoelectric bimorph pointer.

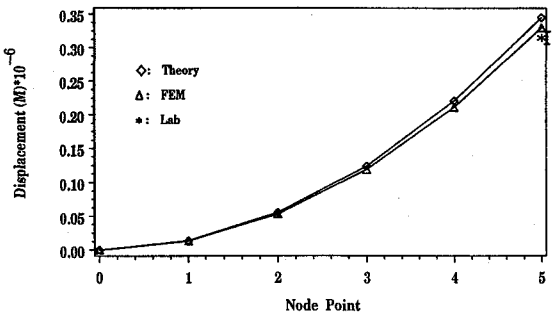

Fig. 4 Static deflection of the bimorph pointer.

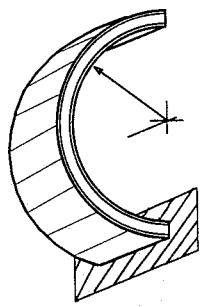

Fig. 5 Laminated semicircular ring shell.

than the theoretical solutions[18] due to inadequate FE modeling. An experimental physical model was also built and tested.[1] The free end displacement (node 5) was measured by a proximeter and plotted in Fig. 4. It is observed that the experiment measurement is slightly lower than the FE calculation due to viscoelastic effect of bonding layers, etc. In addition, nodal displacements based on theoretical and FE calculations (triangular shell element) are also compared with those calculated using an eight-node thin piezoelastic solid FE with a similar mesh density (five elements across).[1] Table 1 summarizes these calculations of five nodal displacements.

Figure 4 and Table 1 suggest that the new piezoelastic triangular shell FE provides rather accurate calculations which compare well with theoretical solutions, experimental data, and thin solid FE solutions. Note that the new triangular shell element is a quadratic element and the thin solid element is a linear element. Accordingly, the shell element predicts better curvature changes along the beam and the error percentages are lower, see Table 1. Other detailed convergence analysis and validations can be found in Ye.[19]

Case 2: Laminated Semicircular Ring Shell

A semicircular steel ring shell is laminated with piezoelectric layers on the top and bottom surfaces, Fig. 5. The steel ring is 100 cm long, 5.08 cm wide, and 0.635 cm thick, and its inner radius is

Table 2 Material properties

Properties	PZT	Steel
Density, ρ, Kg m^{-3}	7.600×10^3	7.750×10^3
Young's modulus, Y, Pa	6.300×10^{10}	6.895×10^{10}
Poisson's ratio, μ	0.300	0.300
Piezostrain constant, d_{31}, m V^{-1}	1.790×10^{-10}	
Electric permittivity, ϵ_{11}, F m^{-1}	1.650×10^{-8}	
Capacitance, C, F m^{-2}	3.080×10^{-6}	

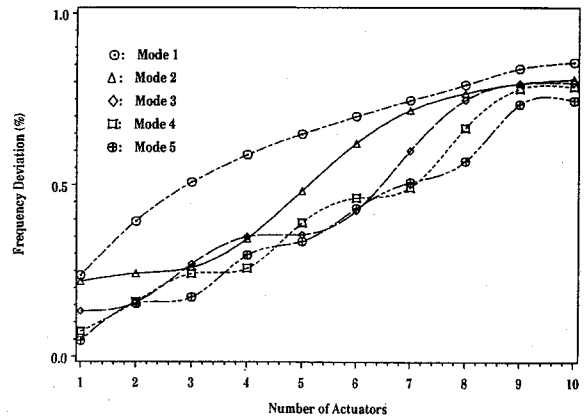

Fig. 6 Percentage of frequency variations of the first five modes.

31.831 cm. The piezoelectric layers are made of lead zirconate titanate (PZT) piezoceramics (254 μm thick). All material properties are provided in Table 2. It is assumed that the inner piezoelectric layer serves as a distributed sensor, the outer layer serves as a distributed actuator, and the bonding layers are not considered.

The ring shell is modeled by 60 triangular shell FEs, 20 for each layer, and 10 element meshes along the ring length. Natural frequencies with and without the influence of piezoelectricity are studied. Distributed vibration control of the ring shell with different lengths of actuators is also investigated and their damping ratios compared. Note that the actuator length is determined by the number of segmented patches measured from the fixed end and the number varies from 1 (segment or patch) to 10 (fully covered).

Free Vibration Analysis

From previous studies, it is known that the inherent piezoelectric effect contributes to the stiffness of a piezoelectric (laminated) structure.[1] There is an additional term associated with the piezoelectric constant and dielectric permittivity appearing in governing electromechanical equations. One purpose of this study is to examine the inherited piezoelectric effect contributed by the length of piezoelectric patches, from 1 (10% covered) to 10 (100% or fully covered) to change the natural frequencies. The first five natural frequencies are 8.17, 25.66, 86.93, 194.14, and 346.08 Hz. Figure 6 shows the frequency variations of the first five natural frequencies when the piezoelectric effect of piezoelectric patches is considered. (Note that the percentage of frequency variations is plotted with respect to the length of the piezoelectric layer, e.g., five patch means half or 50% covered, ten patch means fully or 100% covered, etc.) The percentage change is defined by $(f - f_0)/f_0$ where f and f_0 are natural frequencies of the ring shell with and without piezoelectric effects. It is observed that the percentage of frequency variations appears similar to its mode shape patterns. Longer piezoelectric layers contributes higher deviations from f_0. However, the variations are small, i.e., less than 0.9%. Accordingly, neglecting the piezoelectric effect in eigenvalue calculations does not contribute any significant errors.

An initial damping is assumed to be 0.2%. An initial velocity of 1 m/s is applied to the free end of the ring shell, and the tip responses with and without feedback (negative velocity proportional feedback) control are evaluated. A free vibration time history is plotted in Fig. 7. Note that the beating phenomenon and the higher modes die down quickly. The beating phenomenon is contributed to by the coupling of the first and second mode.

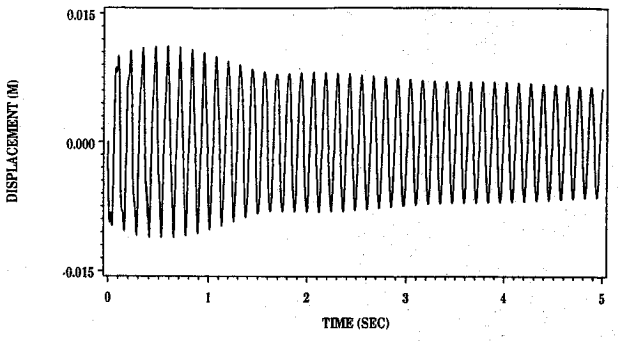

Fig. 7 Free vibration of the ring tip.

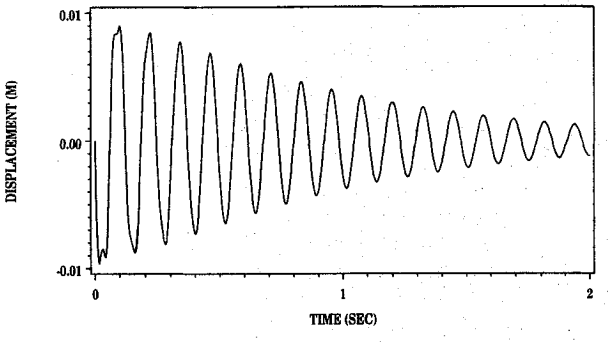

Fig. 8 Controlled response, 2-patch, 20% covered.

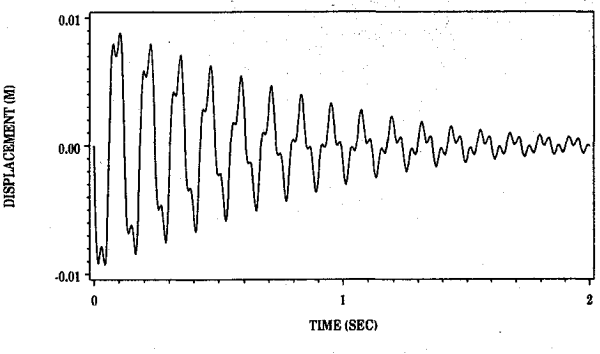

Fig. 9 Controlled response, 5-patch, 50% covered.

Distributed Vibration Control

As discussed earlier, the semicircular ring shell is laminated with a number of segmented distributed actuators, from 1 to 10. [Note that 1 means there is only one piezoelectric actuator patch (10% covered) near the fixed end and 10 means the ring shell is fully covered with 10 pieces of piezoelectric actuator patches; Fig. 5.] The sensor signals from all sensor patches are averaged, amplified, and fed back to all actuator patches. A negative velocity proportional feedback algorithm, no filtering, is used in the analysis.[1] Distributed control effectiveness and controlled damping ratios of the ring shell with different actuator length (measured from the fixed end) are evaluated. Figure 8 shows the free-end controlled response of the semicircular ring shell with a two-patch (20% covered) actuator, Fig. 9 the controlled response of a five-patch (50% covered) actuator, and Fig. 10 the controlled response of a ten-patch (100% or fully covered) actuator. Significant modal coupling between the first and second modes can be observed in Fig. 9. This is due to the control action that also excites the second mode in the feedback-control spillover. Figure 11 summarizes the first-mode controlled damping ratios with different actuator lengths. Note that the fast Fourier transform method and the inverse fast Fourier transform method were used to decouple the first mode response from the multimode coupled response in damping evaluations. It is observed that the controlled damping ratio increases rather quickly from the one-patch actuator to the four-patch actuator, and starts leveling off after the seven-patch actuator (Fig. 11). The maximal control effect is reached at about the seven-patch length actuator.

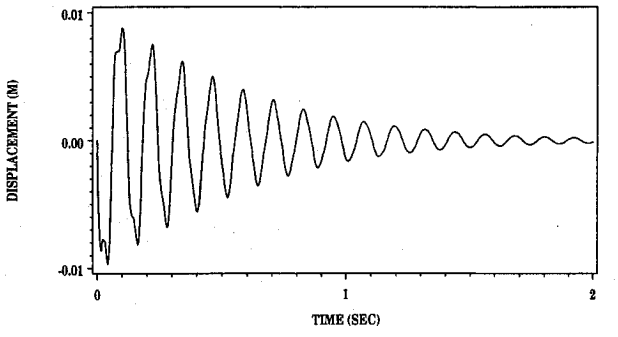

Fig. 10 Controlled response, 10-patch, 100% covered.

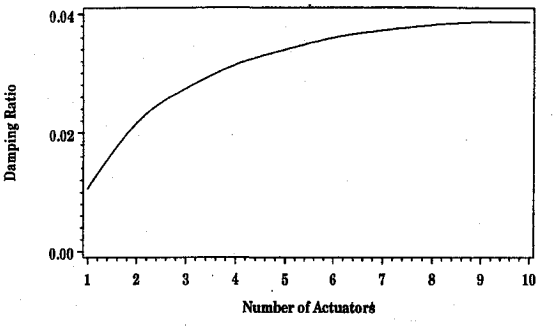

Fig. 11 Damping ratios vs number of actuator patch lengths.

Conclusion

This paper focused on a development of a new laminated piezoelastic triangular shell finite element and its application to piezoelectric laminated systems. Piezoelastic constitutive relations and energy functionals were briefly reviewed. A new laminated quadratic C° piezoelastic triangular shell FE was developed based on the layerwise constant shear angle theory. The new triangular shell element was used to model a piezoelectric bimorph pointer, and its results were closely compared with analytical, experimental, and thin solid piezoelastic FE results.

Then, the triangular shell FE was used to model a semicircular ring shell. The ring shell was laminated with piezoelectric sensor and actuator layers. The length of the sensor/actuator was determined by the number of piezoelectric patches starting from the fixed end, and the number varied from 1 (10% covered) to 10 (100% or fully covered). It was observed that natural frequencies fluctuate when the inherent piezoelectricity in piezoelectric layers is considered; the fluctuation patterns of various piezoelectric lengths follow the mode shape patterns. The percentage errors increase as the piezoelectric layers become longer, however, the maximal deviation is within 0.9%. Accordingly, the piezoelectric effect in eigenvalue analysis can be neglected. Distributed vibration control of the ring shell with different actuator lengths was also studied. Results suggested that the controlled damping ratio increases quickly from the one-patch actuator (10% length) to the four-patch (40% length) actuator, and it levels off at the seven-patch (70% length) actuator. The four-patch (40% length) actuator provides the optimal results when both cost and control effectiveness are considered. Note that bonding layers between laminate are not modeled in these analyses. These layers are viscoelastic in nature, which can influence static deflection as well as dynamic control effects. In practice, however, this bonding layer effect should be minimized in order to maximize the sensing and control effectiveness.

Appendix: Element Matrices

$$\left[M_{uu_j}^{(i)}\right] = \int_{S_j} \left[N_{u_j}(\alpha,\beta)\right]^t \left[\int_{\zeta=0}^{h_i} \left[N_u^{(i)}(\zeta)\right]^t \rho^{(i)} \left[N_u^{(i)}(\zeta)\right] \times B_\alpha^{(i)}(\zeta) B_\beta^{(i)}(\zeta)\, d\zeta \right] \left[N_{u_j}(\alpha,\beta)\right] g_\alpha g_\beta \, d\alpha \, d\beta \qquad \text{(A1)}$$

$$\left[K_{uu_j}^{(i)}\right] = \int_{S_j} \left[B_{u_j}(\alpha,\beta)\right]^t \left[\int_{\zeta=0}^{h_i} \left[B_u^{(i)}(\zeta)\right]^t \left[\bar{c}^{(i)}\right] \left[B_u^{(i)}(\zeta)\right] \times B_\alpha^{(i)}(\zeta) B_\beta^{(i)}(\zeta)\, d\zeta\right] \left[B_{u_j}(\alpha,\beta)\right] g_\alpha g_\beta \, d\alpha \, d\beta \tag{A2}$$

$$\left[K_{u\phi_j}^{(i)}\right] = \int_{S_j} \left[B_{u_j}(\alpha,\beta)\right]^t \left[\int_{\zeta=0}^{h_i} \left[B_u^{(i)}(\zeta)\right]^t \left[\bar{e}^{(i)}\right] \left[B_\phi^{(i)}(\zeta)\right] \times B_\alpha^{(i)}(\zeta) B_\beta^{(i)}(\zeta)\, d\zeta\right] \left[B_{\phi_j}(\alpha,\beta)\right] g_\alpha g_\beta \, d\alpha \, d\beta \tag{A3}$$

$$\left[K_{\phi\phi_j}^{(i)}\right] = -\int_{S_j} \left[B_{\phi_j}(\alpha,\beta)\right]^t \left[\int_{\zeta=0}^{h_i} \left[B_\phi^{(i)}(\zeta)\right]^t \left[\bar{\epsilon}^{(i)}\right] \left[B_\phi^{(i)}(\zeta)\right] \times B_\alpha^{(i)}(\zeta) B_\beta^{(i)}(\zeta)\, d\zeta\right] \left[B_{\phi_j}(\alpha,\beta)\right] g_\alpha g_\beta \, d\alpha \, d\beta \tag{A4}$$

$$\left[K_{\phi u_j}^{(i)}\right] = \left[K_{u\phi_j}^{(i)}\right]^t \tag{A5}$$

$$\left\{F_{u_j}^{(i)}\right\} = \int_{S_j} \left[N_{u_j}(\alpha,\beta)\right]^t \left[N_u^{(i)}(\zeta = h_x)\right]^t \left\{f^{(i)}\right\} B_\alpha^{(i)}(\zeta = h_x) \times B_\beta^{(i)}(\zeta = h_x) g_\alpha g_\beta \, d\alpha \, d\beta + \int_{S_j} \left[N_{u_j}(\alpha,\beta)\right]^t \times \left[\int_{\zeta=0}^{h_i} \left[N_u^{(i)}(\zeta)\right]^t \left\{f_b^{(i)}\right\} B_\alpha^{(i)}(\zeta) B_\beta^{(i)}(\zeta)\, d\zeta\right] g_\alpha g_\beta \, d\alpha \, d\beta \tag{A6}$$

$$\left\{F_{\phi_j}^{(i)}\right\} = -\int_{S_j} \left[N_{\phi_j}(\alpha,\beta)\right]^t \left[N_\phi^{(i)}(\zeta = h_x)\right]^t Q B_\alpha^{(i)}(\zeta = h_x) \times B_\beta^{(i)}(\zeta = h_x) g_\alpha g_\beta \, d\alpha \, d\beta \tag{A7}$$

$$\left[C_{uu_j}^{(i)}\right] = \hat{\alpha}\left[M_{uu_j}^{(i)}\right] + \hat{\beta}\left[K_{uu_j}^{(i)}\right] \tag{A8}$$

where $\hat{\alpha}$ and $\hat{\beta}$ are Rayleigh's coefficients, and

$$B_\alpha^{(i)}(\zeta) = 1 + (\bar{h}_i + \zeta)/R_\alpha \tag{A9}$$

$$B_\beta^{(i)}(\zeta) = 1 + (\bar{h}_i + \zeta)/R_\beta \tag{A10}$$

$$\bar{h}_i = \sum_{k=1}^{i-1} h_k, \qquad \bar{h}_1 = 0.0, \qquad 0.0 \le h_x \le h_i \tag{A11}$$

S_j denotes the area of the triangular shell element in a curvilinear coordinate system.

Acknowledgments

This research was supported, in part, by a grant from the Army Research Office (DAAL03-91-G-0065), Technical Monitor Gary L. Anderson. A fellowship supported by the Center for Computational Sciences at the University of Kentucky is also gratefully acknowledged. The authors are also grateful to anonymous reviewers for their constructive comments and suggestions.

References

[1]Tzou, H. S., *Piezoelectric Shells (Distributed Sensing and Control of Continua)*, Kluwer, Dordrecht, The Netherlands, 1993.

[2]Allik, H., and Hughes, T. J. R., "Finite Element Method for Piezoelectric Vibration," *International Journal of Numerical Methods in Engineering*, Vol. 2, 1979, pp. 151–168.

[3]Nailon, M., Coursant, R. H., and Besnier, F., "Analysis of Piezoelectric Structures by a Finite Element Method," *ACTA Electronica*, Vol. 25, No. 4, 1983, pp. 341–362.

[4]Obal, M. W., "Vibration Control of Flexible Structures Using Piezoelectric Devices as Sensors and Actuators," Ph.D. Thesis, Georgia Inst. of Technology, 1986.

[5]Tzou, H. S., and Tseng, C. I., "Distributed Piezoelectric Sensor/Actuator Design for Dynamic Measurement/Control of Distributed Parameter Systems: a Finite Element Approach," *Journal of Sound and Vibration*, Vol. 138, No. 1, 1990, pp. 17–34.

[6]Ha, S. K., Keilers, C., and Chang, F.-K., "Finite Element Analysis of Composite Structures Containing Distributed Piezoceramics Sensors and Actuators," *AIAA Journal*, Vol. 30, No. 3, 1992, pp. 772–780.

[7]Hwang, W.-S., and Park, H. C., "Finite Element Modeling of Piezoelectric Sensors and Actuators," *AIAA Journal*, Vol. 31, No. 5, 1993, pp. 930–937.

[8]Rao, S. S., and Sunar, M., "Analysis of Distributed Thermopiezoelectric Sensors and Actuators in Advanced Intelligent Structures," *AIAA Journal*, Vol. 31, No. 7, 1993, pp. 1280–1286.

[9]Heyliger, P. R., and Saravanos, D. A., "On Discrete-layer Mechanics for Health-monitoring Applications in Sensor/Active Composite Laminates," *Adaptive Structures and Material Systems*, ASME AD-Vol. 35, American Society of Mechanical Engineers, New York, 1993, pp. 303–312.

[10]Robbins, D. H., and Reddy, J. N., "Analysis of Piezoelectrically Actuated Beams Using a Layer-wise Displacement Theory," *Computers and Structures*, Vol. 41, 1991, pp. 265–279.

[11]Tzou, H. S., and Ye, R., "Piezothermoelasticity and Precision Control of Piezoelectric Systems," *Journal of Vibration and Acoustics*, Vol. 116, No. 4, 1993, pp. 489–495.

[12]Pervez, T., and Zabaras, N., "Transient Dynamic and Damping Analysis of Laminated Anisotropic Plates Using a Refined Plate Theory," *International Journal of Numerical Methods in Engineering*, Vol. 33, 1992, pp. 1059–1080.

[13]Reddy, J. N., "A Penalty Plate-bending Element for the Analysis of Animated Anisotropic Composite Plates," *International Journal of Numerical Methods in Engineering*, Vol. 15, 1980, pp. 1187–1206.

[14]Kwon, Y. W., and Akin, J. E., "Analysis of Layered Composite Plates Using a High-order Deformation Theory," *Computers and Structures*, Vol. 27, 1987, pp. 619–623.

[15]Seide, P., and Chaudhuri, R., "Triangular Finite Element for Analysis of Thick Laminated Shells," *International Journal of Numerical Methods in Engineering*, Vol. 24, 1987, pp. 1563–1579.

[16]Tzou, H. S., and Bao, Y. "Modeling of Thick Anisotropic Composite Triclinic Piezoelectric Shell Transducer Laminates," *Journal of Smart Materials and Structures*, Vol. 3, 1994, pp. 285–292.

[17]Zienkiewicz, O. C., and Taylor, R. L., *The Finite Element Method*, 4th ed., Vol. 1, Basic Formulation and Linear Problems, McGraw–Hill, New York, 1989.

[18]Tzou, H. S., "Development of a Light-weight Robot End-effector using Polymeric Piezoelectric Bimorph," *Proceedings of the 1989 IEEE International Conference on Robotics and Automation*, 1989, pp. 1704–1709.

[19]Ye, R., "Active Piezothermoelastic Composite Systems: Finite Element Development and Analysis," Ph.D. Dissertation, Dept. of Mechanical Engineering, Univ. of Kentucky, Lexington, KY, 1995.